

**“TREATING COAL-BED METHANE PRODUCED WATER FOR
BENEFICIAL USE BY MFI ZEOLITE MEMBRANES”**

ANNUAL TECHNICAL REPORT

REPORTING PERIOD START DATE: October 1, 2004

REPORTING PERIOD END DATE: September 30, 2005

PRINCIPAL INVESTIGATOR:

Junhang Dong, Ph.D.
Petroleum Recovery Research Center
Petroleum & Chemical Engineering Department
New Mexico Institute of Mining and Technology
801 Leroy Place, Socorro, NM 87801
Phone: (505) 835-5293; Fax: (505) 835-5210; Email: jhdong@nmt.edu

PROJECT MANAGER:

Robert Lee, Ph.D.
Petroleum Recovery Research Center
New Mexico Institute of Mining and Technology
801 Leroy Place, Socorro, NM 87801
Phone: (505) 835-5408; Fax: (505) 835-6031; Email: Lee@prrc.nmt.edu

DATE REPORT WAS ISSUED: December 2005

DOE AWARD NUMBER: DE-FC26-04NT15548

DISCLAIMER:

This report was prepared as an account of work sponsored by an agency of the United States Government. Neither the United States Government nor any agency thereof, nor any of their employees, makes any warranty, express or implied, or assumes any legal liability or responsibility for the accuracy, completeness, or usefulness of any information, apparatus, product, or process disclosed, or represents that its use would not infringe privately owned rights. Reference herein to any specific commercial product, process, or service by trade name, trademark, manufacturer, or otherwise does not necessarily constitute or imply its endorsement, recommendation, or favoring by the United States Government or any agency thereof. The views and opinions of authors expressed herein do not necessarily state or reflect those of the United States Government or any agency thereof.

ABSTRACT

Coal-bed methane (CBM) and Oilfield produced water is a growing environmental problem, which limits the highly demanded increase in gas and oil production. At present, produced water is mainly disposed by costly deep-well injection, which adds a significant financial burden to the industry. In the southwest arid areas, a proactive strategy for produced water management is to retrieve clean water for beneficial use and minimize the volume of concentrated brine for final disposal. Unfortunately, current technologies are either technically incapable of or economically inefficient for desalinizing the organic-containing, high concentration produced waters.

This three-year project aims to develop a new technology of reverse osmosis through molecular sieve zeolite membranes to efficiently treat the high TDS (total dissolved salts) CBM produced water for beneficial use. The main objective of Year 1 (Phase I) research is to understand the mechanism of reverse osmosis (RO) on zeolite membranes and factors determining the separation performance. In the past year, defect-free MFI-type and FAU-type zeolite membranes have been successfully synthesized on porous alumina discs and tubular substrates by in-situ hydrothermal crystallization and by seeding secondary growth methods. Extensive experiments have been performed to investigate water and ion transport mechanisms in the MFI zeolite membranes during RO. The effects of operation temperature, pressure, and feed chemical composition on the RO performance were studied. Based on the experimental data, a phenomenological mass transport model has been established for the RO process on zeolite membranes. All major tasks and objectives proposed in the “Statement of Work (SOW)” for the first project year have been accomplished in time. The results obtained in this year have built a solid base for continuing the research work in Phase 2.

TABLE OF CONTENTS

DISCLAIMER	1
ABSTRACT	2
TABLE OF CONTENTS	3
EXECUTIVE SUMMARY	4
TECHNICAL REPORT	6
1. Synthesis of defect-free zeolite membranes	6
1.1. Synthesis Methods	6
<i>MFI membrane synthesis</i>	6
<i>FAU membrane synthesis</i>	7
1.2. Results and Discussion	8
<i>MFI zeolite membranes</i>	8
<i>FAU zeolite membranes</i>	11
1.3. Conclusions	12
2. Mass transport mechanisms in zeolite membranes during RO processes and effects of operating conditions	12
2.1. Mechanism of RO on zeolite membrane	13
2.2. Experimental methods	14
2.3. Results and discussions	15
<i>Effect of temperature</i>	17
<i>Effect of ion charge density</i>	17
<i>Effect of pressure</i>	18
<i>Modeling and analysis</i>	20
<i>Effect of dissolved organics</i>	27
<i>Sensor for produced water management</i>	28
2.4. Conclusions	29
REFERENCES	30
PUBLICATIONS IN YEAR1	31

EXECUTIVE SUMMARY

Coal-bed methane (CBM) and Oilfield produced water is a growing environmental problem, which limits the highly demanded increase in gas and oil production. Direct release of produced water containing a high concentration of dissolved salts and organics contaminates soil and the ground and surface water systems. Currently, produced water is mainly disposed by costly deep-well injection, which adds a significant financial burden to the industry. Additionally, freshwater shortage is a major constraint for economic development in many southwest arid states producing oil and gas. Therefore, in these arid areas, a proactive strategy for produced water management is to retrieve clean water for beneficial use and minimize the volume of concentrated produced brine for final disposal. Unfortunately, current technologies, such as polymeric membrane reverse osmosis (RO), distillation, and ion exchange, are either technically incapable of or economically inefficient for desalinating the organic-containing, high concentration produced waters.

This three-year project aims to develop a new technology of reverse osmosis through molecular sieve zeolite membranes to efficiently treat the high TDS (total dissolved salts) CBM produced water for beneficial use. The main objectives for the first project year include (1) to synthesize high quality zeolite membranes on practical substrates, (2) to understand the mechanisms of the RO desalination process on zeolite membranes, and (3) identify factors determining the membrane performance in terms of ion rejection and water flux rates. The major tasks and objectives proposed in the SOW for Year 1 have been fulfilled on schedule.

Defect-free MFI-type zeolite membranes (pore size 0.56nm) were successfully synthesized on both porous alumina discs and tubular substrates mainly by in-situ crystallization. Defect-free FAU Y-type zeolite membranes (pore size 0.74nm) were synthesized on the disc and tubular substrates by the seeding-secondary growth method. The reverse osmosis experiments have been performed on both the disc-shaped and tubular membranes. The FAU membranes were found to be less effective for RO desalination in terms of ion rejection compared to the MFI-type membranes. Mechanistic studies have been conducted to understand the effects of ion size, temperature, and hydraulic pressure on the water/ion transport behavior in the MFI membranes. The experimental data was interpreted using a classic model by taking into account the distinct interactions between ion, water, and zeolite surface.

The ion rejection in MFI-type membranes was found to depend primarily on the size selectivity of the hydrated ions which is larger than the zeolite pore size. Excellent rejection rates can be obtained for ions of high charge density in a wide range of concentration. Ions with relatively low charge density can be partially dehydrated at the membrane surface to enter and transport through the zeolite channels, resulting in reduced ion rejection rates. In general, the ion and water fluxes can be enhanced simultaneously by increasing the temperature or the transmembrane pressure (ΔP). However, changing temperature and pressure have different impacts on the ion reject rate. Raising temperature has a greater influence on the ion permeation than on the water permeation, resulting in a slight decline of the ion rejection. On the contrary, increasing the transmembrane pressure can enhance both the water flux and ion rejection because the ion flux is much less affected by pressure than is the water flux. Thus, optimization of the operating conditions is essential for enhancing the RO performance, i.e. water flux and ion rejection.

The zeolite membrane also showed high rejection rates for dissolved organics (>99% for ~500 ppm toluene) during the RO process. However, the presence of dissolved organics in the feed solution decreased the water flux and ion rejection rates because of the adsorption of organic molecules into the zeolite pores. The currently used MFI membranes synthesized from an Al-free precursor were basically hydrophobic silicalite, which is a strong adsorbent for organics. However, the membranes fouled by organics can be effectively regenerated by simple thermal treatment at >250°C. The separation performance was improved on hydrophilic ZSM-5 (MFI-type with Si/Al ratio ~50) membranes.

For effective produced water management, cheap analytical technologies (e.g. chemical sensors) for fast, in situ, and real-time monitoring of the chemicals in water and gas phases are highly demanded. Unfortunately, such chemical sensors are currently unavailable. In this research, a new type of MFI zeolite film-integrated optical fiber sensors has been developed for in-situ detection of organics in water and gas phases. The sensors operate by monitoring the optical reflectivity changes caused by the selective adsorption of organic molecules from aqueous solutions or gases in the zeolitic pores.

The research results obtained in Year 1 (Phase I) demonstrated that zeolite membranes are capable of purifying produced brines. The outstanding chemical, structural, and thermal stabilities of the zeolite materials make the zeolite membranes suitable for treating the organic containing CBM produced water. At present, for feed solutions with TDS of 6,000 ~ 18,000 ppm, the typical water flux and ion rejection rates of the MFI membranes are 0.5~0.8kg/m²·hr and 85~99%, respectively, under relatively low operating pressures of ~ 400 psi. The ion rejection was found to decrease with increasing the TDS level because of the effect of the less selective nano-scale intercrystal pores. In Phase II (Year 2) of the project, research will focus on membrane modification for high-TDS produced water treatment and optimization of operating conditions to enhance water flux and ion rejection.

TECHNICAL REPORT

1. Synthesis of defect-free zeolite membranes

1.1. Synthesis Methods

MFI membrane synthesis: MFI zeolite membranes were synthesized by in-situ crystallization on the inner surfaces of tubular α -Al₂O₃ substrates (Pall Corp., New York, USA). The alumina tube was 8 cm in length with inner and outer diameters of 7 mm and 10 mm, respectively. The two ends of the tube were coated with glass sealing layers. The bore side top layer of the tubular substrate had an average pore size of 0.2 μ m and a porosity of 35~40%. Chemicals used in this study included NaOH pellets (99.99%, Aldrich), fumed SiO₂ (99.98%, Aldrich), 1M tetrapropylammonium hydroxide (TPAOH) solution (Aldrich), p-xylene (99%, Aldrich), m-xylene (99%, Aldrich), o-xylene (98%, Sigma-Aldrich), benzene (99.9%, Aldrich), toluene (Fisher, 99.8%), ethylbenzene (99.8%, Aldrich), nonane (99%, Sigma) and deionized (DI) water. High purity helium (99.99%), hydrogen (99.99%) and methane (99.97%) were obtained from Matheson Tri-Gas, Inc.

The zeolite synthesis solution was obtained by dissolving 0.49 g NaOH pellets and 7 g fumed SiO₂ in 35 ml of 1M TPAOH solution. In this work, the following process was developed for synthesizing high quality tubular MFI membranes. The visually clear synthesis solution was filtered by filter paper (20~30 μ m) before use. This filtration step was found to greatly improve the membrane quality and reproducibility of membrane production. The filtered synthesis solution was then transferred into a cylindrical autoclave with chamber diameter and length of 2 cm and 10.5 cm, respectively. The amount of synthesis solution in the autoclave was at such a level that the substrate tube was fully immersed in the solution when it was placed horizontally

on a roller installed in a temperature-programmable oven. The roller was driven by a transmission gear.

Hydrothermal synthesis was carried out at 180°C for 20 h. During the synthesis, the cylindrical autoclave was rotated about its axes at a speed of three revolutions per minute. After the hydrothermal synthesis, the membrane tube was washed and dried. The membrane was then fired in air at 450°C for 8 h with a heating rate of 0.3 °C/min and a cooling rate of 0.5 °C/min. The membranes received a second hydrothermal treatment following the above procedure to improve the membrane density. A dense MFI zeolite membrane was formed on the inner surface of the tube but no zeolite coating was found on the outer surface, likely due to the attrition between the tube surface and the autoclave wall during the rotating synthesis process.

FAU membrane synthesis: Faujasite (FAU) zeolite membranes were prepared by a seeding and secondary growth approach. Disc-shaped porous α -Al₂O₃ substrates, 2-mm thick, 29-mm in diameter, with a mean pore size of about 0.10 μ m and porosity of 30-35%, were seeded with FAU (NaY) zeolite crystals with size of 1 – 1.5 μ m. The above described tubular substrates were also used to form NaY membrane on the inner side. The NaY seed particles were synthesized from an aluminosilicate gel with molar composition of 12.8 SiO₂ : 1 Al₂O₃ : 17 Na₂O : 675 H₂O. The temperature and time for hydrothermal synthesis of the seed particles were 90°C and 12 h. The substrates were seeded by dip coating with suspensions of zeolite NaY crystals. The zeolite seed suspension for dip coating was prepared by dispersing 0.1 g of the synthesized NaY powders in 25 ml D.I. water. The pH value of the suspension was adjusted to 3~4 by adding 1.0 M HNO₃ solution. The suspension was stirred rigorously for 24 h before use. After dip coating,

the coated discs were dried at 60°C in air for 24 h.

The aluminosilicate gel used for secondary growth had a composition of 10.7 SiO₂: 1 Al₂O₃: 18.8 Na₂O: 850 H₂O. The synthesis gel was prepared by mixing water glass (27%SiO₂ + 14%NaOH, Aldrich), sodium aluminate (50-56%Al + 40-45%Na (Fe<0.05%), Riedel-deHaen), and sodium hydroxide (99.99%, Aldrich). The gel was rigorously stirred for 12 h and poured into an autoclave, where a substrate was mounted horizontally on a stand with its seeded side facing downward. Hydrothermal crystallization was carried out at 85~105°C in the closed autoclave for 3 to 24 h. The hydrothermal treatment was repeated to minimize the intercrystal pores. The synthesized membranes were washed with D.I. water and then dried at 60 °C in air for at least 24 h before any tests or characterizations.

1.2. Results and Discussions

MFI zeolite membranes: Defect-free MFI-type zeolite membranes (pore size 0.56nm) have been synthesized on both porous alumina discs and tubular substrates by in-situ crystallization and seeding-secondary growth methods. High quality FAU Y-type zeolite membranes (pore size 0.74nm) were also synthesized by the seeding-secondary growth technique.

Fig. 1 shows the scanning electron microscopic (SEM) images of the tubular MFI zeolite membrane. The thickness of the zeolite membrane was about 2µm according to the SEM observation. Fig. 2 is the X-ray diffraction (XRD) patterns of the zeolite particles collected from the residual solution and the tubular membrane. The XRD patterns indicate a pure MFI phase on the α-alumina substrate. BET measurements were conducted for both the zeolite particle and supported membrane samples using nitrogen as a probe gas. The powder sample had a BET

surface area of $394.0339 \pm 4.9420 \text{ m}^2/\text{g}$ with a micropore volume of $\sim 0.1435 \text{ cm}^3/\text{g}$, which were virtually the same as the literature values of silicalite. The membrane sample, which contained part of the substrate, had a BET surface area of $11.8506 \pm 0.1294 \text{ m}^2/\text{g}$ and a micropore volume of $0.0045 \text{ cm}^3/\text{g}$. The ratios of (BET surface area)/(micropore volume) were similar for the powders ($2745.9 \text{ m}^2/\text{cm}^3$) and the membrane ($2633.5 \text{ m}^2/\text{cm}^3$). For both samples, the micropore size was measured to be 5.8 \AA . The supported membrane had a micropore/mesopore volume ratio of $\sim 7:1$ with a mesopore size distribution from 26 to 38 \AA . However, this micropore/mesopore ratio might not represent the true value in the active membrane layer because the microstructure is not uniform along the thickness of the zeolite membrane, especially in the zeolite/substrate interface region and the membrane outer surface.

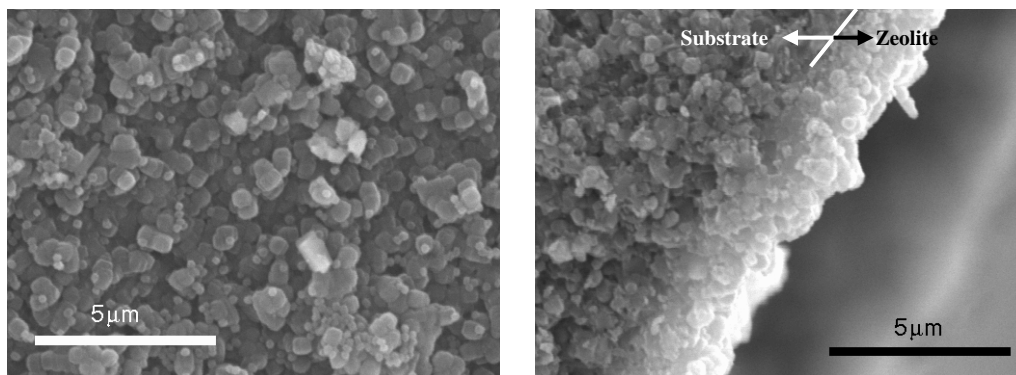


Fig. 1 SEM pictures of the tubular MFI membrane (left – surface; right – cross-section).

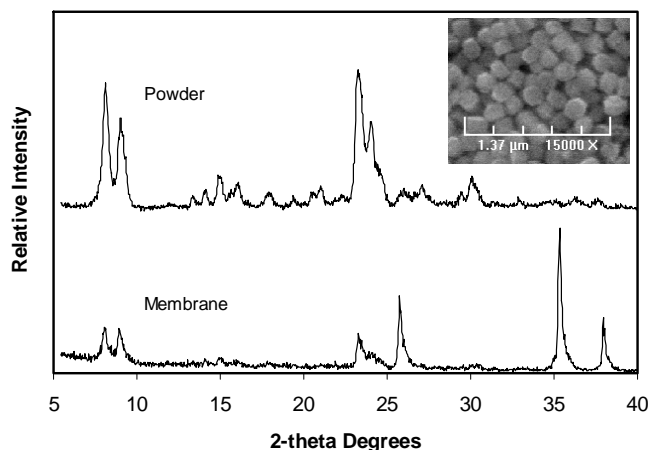


Fig. 2 XRD patterns of the MFI zeolite powders and membrane (insert: MFI particles).

The quality (integrity) of the MFI membranes was examined by separation of p-xylene (PX) and o-xylene (OX) vapors because successful separation of these two isomers requires a minimization of intercrystal pores and elimination of any micro-defects in the membrane. The PX/OX vapor mixture was carried by helium and fed to the outer side of the tube. The partial pressures of PX and OX in the feed were 0.52 kPa and 0.39 kPa, respectively. Pure helium swept the inner surface (zeolite membrane) of the tube. The xylene permeance and separation factor are presented as functions of operation temperature (70-300°C) in Fig. 3. The data at each temperature were collected after stabilizing for at least 6 h. The permeance and perm-selectivity values measured from permeation of pure PX and OX vapors are also included in Fig. 3 for comparison. A maximum PX/OX separation factor of about 17.8 was obtained for the binary mixture at 250°C, with p-xylene permeance of 9.5×10^{-9} mol/m²·s·Pa while the maximum PX/OX perm-selectivity of 72.9 was observed at ~ 150°C. These very high separation factor and perm-selectivity values indicated that membranes are of high quality. More detailed information and relevant references are available in a recent publication [1].

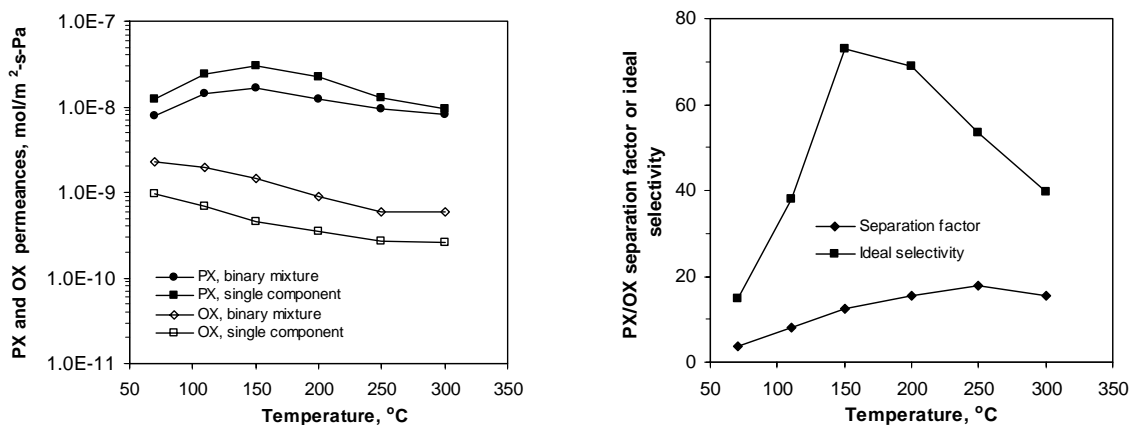


Fig. 3 Single-component and binary permeation of p/o- xylenes vs. temperature.

FAU zeolite membranes: After optimizing the synthesis conditions, including the seeding approach, gel composition, and hydrothermal treatment process, defect-free, pure NaY type zeolite membranes have been successfully synthesized. The quality of the membrane was evaluated by separation of equimolar CO₂/N₂ mixtures. At room temperature, the CO₂ selectivity was above 30 for the CO₂/N₂ dry gas mixture with a CO₂ permeance of 2.1x10⁻⁸ mol·m⁻²·Pa⁻¹·s⁻¹. These indicated that the membranes were free of defects. Fig. 4 and Fig. 5 show the microscopic images and XRD patterns of the FAU zeolite, respectively. More detailed information and relevant references are available in recent publications [2,3].

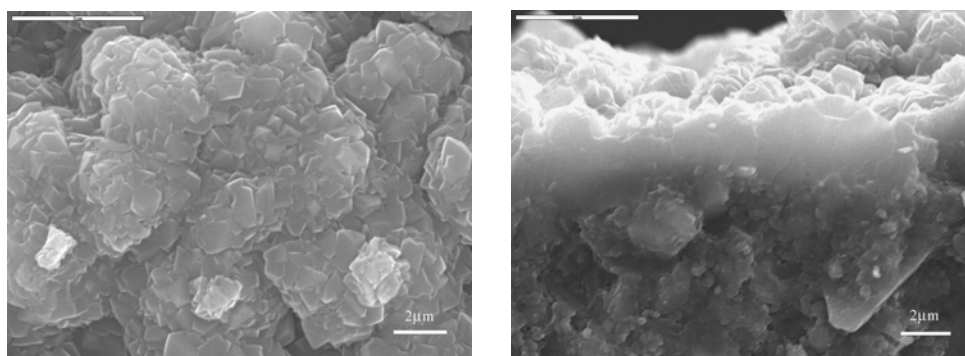


Fig. 4 SEM pictures of membrane M_{4,6}. (Left) surfaces, (right) cross section.

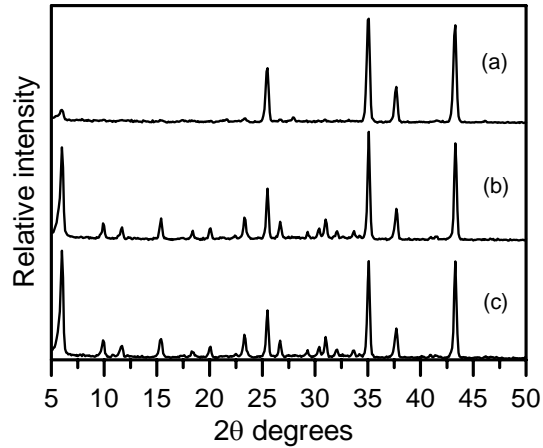


Fig. 5 XRD patterns of FAU zeolite membranes synthesized from gels with different Si/Al ratios. Synthesis gels: (a) Si/Al = 9.6, (b) Si/Al = 6.4, (c) Si/Al = 5.4.

1.3. Conclusions

MFI-type and FAU-type zeolite membranes have been synthesized on porous α -alumina discs and commercial tubular alumina supports (Pall Co.). The synthesis methods developed in this work provide high reproducibility for membrane production. Both the MFI and FAU membranes were of high quality as indicated by the excellent gas separation performance. The next step of research on membrane synthesis will focus on further reducing the membrane thickness so that the mass transport resistance can be reduced and the water flux can be enhanced in the RO process.

2. Mass transport mechanisms in zeolite membranes during RO processes and effects of operating conditions

2.1. Mechanism of RO on zeolite membranes

Rejection rates of multivalent cations (e.g. Ca^{2+} , Mg^{2+} , and Al^{3+}) and anion SO_4^{2-} were found to be extremely high (>99%) on MFI membranes due to their high charge density and large dynamic hydration numbers [4,5]. Therefore, research has been focused mainly on the univalent ions (i.e. alkaline metal ions).

The pure-silica zeolites do not contain cation compensators; hence they have no ion exchange capacities. In perfect PSZ membranes, the uniform subnanometer zeolitic pores are sufficiently large for water molecules (dynamic size $\sim 3.0 \text{ \AA}$) to diffuse through but small enough to restrict the entry and transport of hydrated ions. The molecular dynamic (MD) simulation indicated that PSZ ZK-4 zeolite membranes (pore diameter $\sim 4.2 \text{ \AA}$) could achieve nearly 100% rejection of Na^+ during RO of its aqueous solutions. Such a perfect ion separation is achievable only on single crystal PSZ membranes with pore size significantly smaller than the dynamic size of hydrated ions. The size selectivity for cations has also been shown by potentiometric analysis on silicalite (i.e. PSZ MFI), sodalite, NaA, and NaY zeolite polycrystalline films. The ion rejection rate (r_i) on the MFI membranes was found to depend on the ion charge density, defined as the electrical charge per volume of the ion, because the charge density determines the number of tightly bound water molecules and the dynamic size of the hydrated ion.

For MFI zeolite membranes, ions with fewer tightly bound water molecules and smaller dynamic sizes may be able to enter and diffuse through the zeolitic pores. Moreover, cation sorption can occur on the negatively charged surface of the all-silica MFI zeolite, which may cause ion transfer through surface diffusion under a gradient of ion surface coverage along the channels. In polycrystalline zeolite membranes, ions can also permeate through the inherent intercrystal pathways. The average size of the intercrystalline pores is normally in a range of 1 –

3 nm in MFI type zeolite membranes of reasonably good quality. These nanoscale intercrystal spaces are the major cause for the decline of separation efficiency, especially for separations relying on a molecular sieving mechanism.

The effect of intercrystalline pores on the ion separation in zeolite membranes depends on the ionic strength of the feed solution [6]. When in contact with aqueous solutions, an electrically charged double-layer forms at the surface of the zeolite crystal. The thickness of the double layer decreases as the ion concentration increases. In solutions of low ion concentrations, the charged double layers can overlap in the nano-scale intercrystalline space, which effectively limits the entry and motion of charged ions. Therefore, for high quality zeolite membranes, the ion permeation through a very small number of intercrystal pores may be negligible during RO of dilute solutions. Under very high ion concentrations, the double layers may be reduced to the thickness of Helmholtz layer ($a/2 \approx 0.1$ nm) which opens up the intercrystal pores, allowing ions to permeate with less resistance, and thus significantly lowers the ion rejection rate.

For the development of zeolite membranes for RO desalination, understanding of the ion transport behavior in zeolite membranes is of critical importance. Unfortunately, prediction of ion rejection and ion diffusion rates (F_i) in zeolite membranes is currently difficult because of the complexities of the zeolite material chemistry, membrane microstructure, and the ion-water and ion-zeolite surface interactions. The lack of experimental data of ion and water permeation through zeolite membranes has also hindered the advancement of theoretical models. In this study, ion rejection and ion and water flux rates through MFI zeolite membranes were determined for alkali metal ions through RO of 0.1 M solutions of their chlorides.

2.2. Experimental methods

The RO experiments were conducted by a cross-flow operation with the zeolite membrane surface and the substrate facing the feed solution and the permeate side, respectively. The membrane disc was mounted in a stainless steel cell, which was immersed in a water bath ($\pm 0.2^\circ\text{C}$, RDL 20, GCA) for temperature control. The feed solution was stored in a stainless steel reservoir, which was pressurized by a nitrogen cylinder. When the tubular membrane was used, the feed stream went through the bore side and the permeate stream flowed in the shell side. All the RO experiments on the disc shaped membrane were conducted with a feed pressure of 2.75 MPa. The feed flow rate was controlled by a needle valve located at the exit of the feed chamber. The permeate side was at atmospheric pressure (87 kPa in the lab). Each permeate sample was collected for 12 hours. Both the cation (M^+) and anion (Cl^-) concentrations of the permeate solutions were analyzed by a dual-column ion chromatograph (IC, DX120, Dionex).

The RO experiments were first carried out for the 0.1 M LiCl solution at 10, 30, 50, and 60°C . The membrane was then used to measure the RO data for the 0.10 M single-salt solutions of other alkali metal chlorides including KCl, RbCl and CsCl at 50°C . Finally, RO experiments were conducted for the 0.1 M NaCl solution at 10, 30 and 50°C . Between the experiments for different solutions, the membrane was washed thoroughly with DI water and the solution to be tested next. The RO experiments were also performed on tubular MFI membranes for the 0.1M NaCl solution to study the effect of transmembrane pressure on ion and water transport at room temperature (23°C).

2.3. Results and discussions

The cation/anion molar ratio in the permeate solution was found to be consistent with the stoichiometric ratio of the chlorides ($\text{M}^+:\text{Cl}^- = 1:1$). The pH of the permeate solution was found

to be slightly higher than that of the feed solution which was probably caused by the concentration difference between the feed and permeate. For example, the pH values of a 0.1M NaCl feed and a ~0.01M NaCl permeate were found to be 6.04 and, 6.58 respectively, which compared well with the pH values of freshly prepared 0.1M (pH=6.09) and 0.01 M (pH=6.43) NaCl solutions. These indicated cation-anion paired permeation through the membrane that maintained the electrical neutrality [4]. The concentration of the feed solution was treated as constant in data processing because the permeate flow rates were less than 1.0% of the feed flow rates. The flux (J_i) and rejection (r_i) rates of component i , are defined by

$$J_i = \frac{Q_i}{A_m \cdot \varepsilon \cdot t} \quad (1)$$

where Q_i is the moles of ion ($i = Li^+, Na^+, K^+, Rb^+, Cs^+$, or w for water) collected in a time period of t ; A_m is the straightforward membrane area; and ε is the porosity of the substrate; and

$$r_i = \frac{C_{i,f} - C_{i,p}}{C_{i,f}} \quad (2)$$

where $C_{i,f}$ and $C_{i,p}$ are concentrations of ion i in the feed and permeate solutions, respectively (mol/m^3). For dilute solutions, the overall ion selectivity of the membrane (α_i) is given by

$$\alpha_i = \frac{x_p / (1 - x_p)}{x_f / (1 - x_f)} \approx \frac{x_p}{x_f} \approx \frac{C_{i,p}}{C_{i,f}} = 1 - r_i \quad (3)$$

where x_f and x_p are mole fractions of ion in the feed and permeate solutions, respectively; and $C_{i,f}$ and $C_{i,p}$ are ion concentrations in the feed and permeate solutions, respectively.

Effect of temperature: Table 1 summarizes the results of RO for the 0.1 M LiCl and 0.1 M NaCl single-salt solutions at different temperatures. For both LiCl and NaCl solutions, raising the temperature increased the water and ion fluxes and decreased slightly the ion rejection rates.

Table 1. Results of RO for the 0.1M LiCl and 0.1 M NaCl solutions

T, °C	0.10 M LiCl			0.10 M NaCl		
	r_{Li+} , %	J_{Li+} mol·m ⁻² ·h ⁻¹	J_w mol·m ⁻² ·h ⁻¹	r_{Na+} %	J_{Na+} mol·m ⁻² ·h ⁻¹	J_w mol·m ⁻² ·h ⁻¹
10	99.3	1.50×10^{-4}	11.9	98.2	3.23×10^{-4}	13.0
30	99.0	2.30×10^{-4}	12.8	98.0	6.80×10^{-4}	18.9
50	98.8	4.26×10^{-4}	19.7	97.8	8.52×10^{-4}	21.5
60	98.7	5.60×10^{-4}	23.9			

Effect of ion charge density: Figures 6 and 7 show the ion rejection rates and water and cation fluxes as functions of the crystallographic ion size at 50 °C, respectively. The ion rejection rate decreased with increasing crystallographic ion size as shown in Figure 6. The ion flux increased with ion crystallographic size monotonically from J_{Li+} (4.26×10^{-4} mol/m²·h) to J_{Cs+} (1.90×10^{-3} mol/m²·h). The water flux exhibited a trend of increasing then decreasing as a function of the alkali metal ion (size) in the solutions with a maximum flux appearing for the 0.1 M KCl solution.

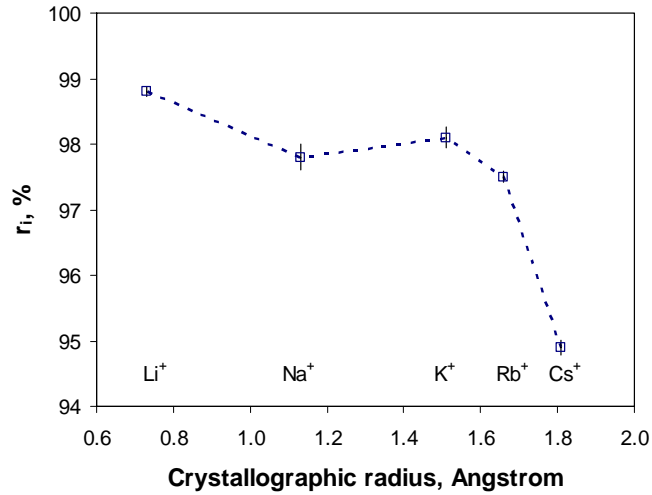


Fig. 6 Rejection rates of alkali metal ions on the MFI membrane at 50 °C.

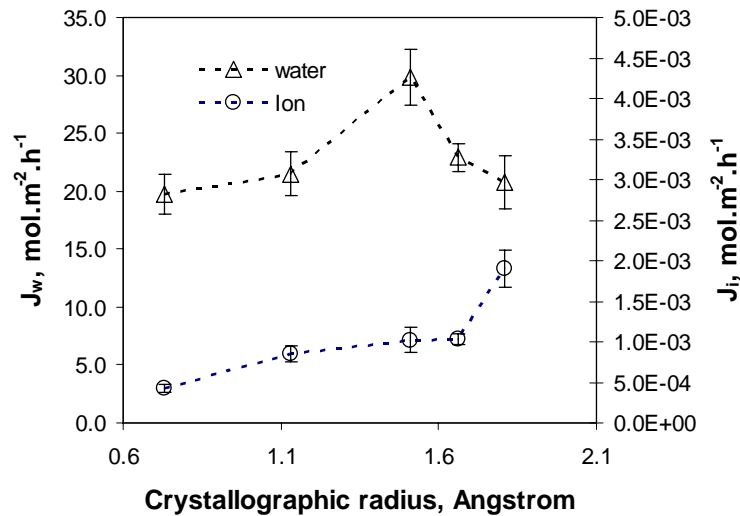
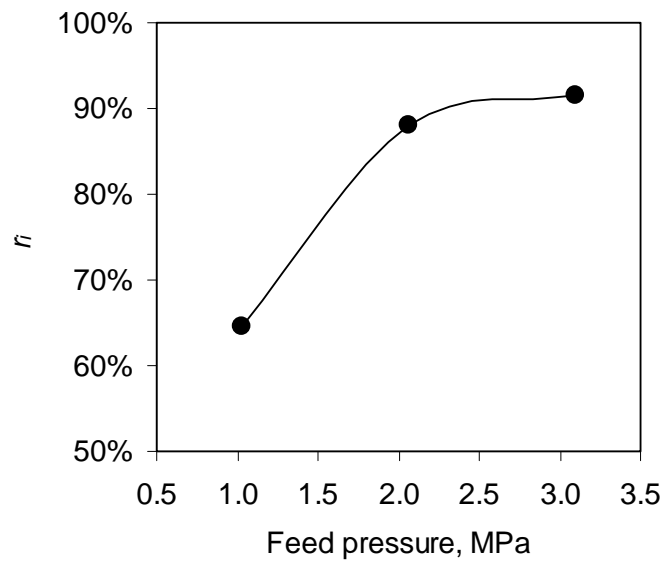


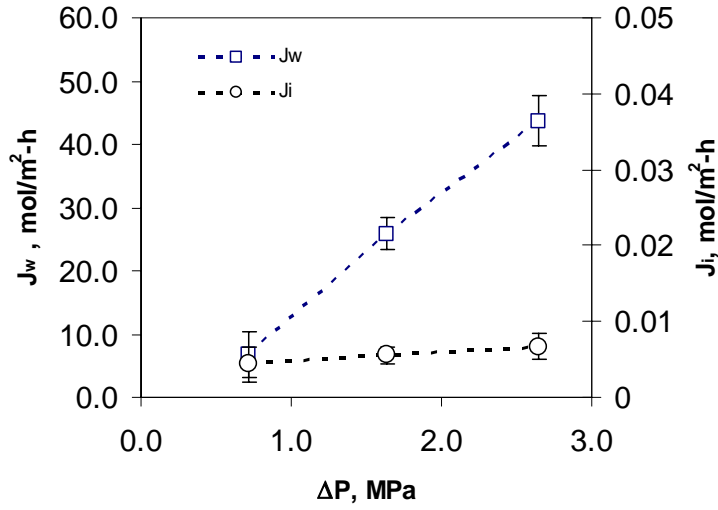
Fig. 7 Ion and water fluxes as functions of ion size at 50 °C.

Effect of pressure: Figure 8 shows the results of RO on the tubular membrane for 0.1 M NaCl solution under different feed pressures. The Na^+ rejection rate increased continuously with increasing the feed pressure. Both the ion and water fluxes were found to increase linearly with

the transmembrane pressure ($\Delta P = P_f - P_p - \Delta\pi$). P_f and P_p are pressures of the feed and permeate sides, respectively, Pa ; and $\Delta\pi$ ($\approx RT[C_{i,f} - C_{i,p}]$) is the osmosis pressure difference between the feed and permeate solutions, Pa . However, the magnitude of increase in the water flux was much greater than that in the ion flux. When ΔP rose from 0.71 to 2.65 MPa, the J_w was enhanced by more than five times but J_i was increased by only about 54%. The non-proportional increase in the water and ion fluxes indicated that water molecules could surpass the Na^+ inside the zeolite channel.



(a)



(b)

Fig. 8 Na⁺ rejection (a) and water and Na⁺ fluxes (b) as functions of feed pressure (or ΔP).

Modeling and analysis: In the traditional nonporous RO membranes, the water flux is a function of transmembrane pressure ΔP and the ion flow rate is determined by a pressure-independent solution-diffusion mechanism.

$$J_w = -K_w \cdot \frac{dp}{d\delta} = K_w \cdot \frac{[P_f - P_p - \Delta\pi]}{\delta} = K_w \frac{\Delta P}{\delta} \quad (4)$$

Where K_w is the membrane permeability ($mol/m \cdot s \cdot Pa$) for water, and δ is the membrane thickness. $K_w = k_w D_w = k_w D_w^0 \cdot \exp(-\Delta E_w / RT)$, where k_w can be considered as water solubility (loading) in the zeolite ($mol/m^3 \cdot Pa$) and D_w is water diffusivity (m^2/s). Therefore, increasing the feed pressure enhances the water flux and ion rejection but does not affect the ion flux if change in concentration polarization is negligible.

The zeolite membrane has a subnanometer porous structure which is different from that of the nonporous polymer membranes. The linear pressure-dependence of the water flux in the zeolite membrane can also be described by eq. (4) but the ion flux in the zeolite membrane may not be approximated to be pressure-independent as it often is for the nonporous membranes. The MD simulations have shown that water molecules and hydrated ions can pass by each other in the MFI-like channels [7]. Due to the space confinement in the subnanometer channels and the strong interaction between the ion, water molecule, and pore surface, the ion and water mobilities are mutually affected. Therefore, the pressure-dependence of the ion flux likely resulted from the enhanced ion diffusion (ions are dragged by the fast moving water) in the zeolite channels and also from the possibly increased concentration polarization under higher water flux.

The molecular transport through a zeolite membrane is often considered a five-step process that includes (i) diffusing from the bulk feed to membrane surface, (ii) entering the zeolitic pores from the membrane surface, (iii) diffusing through the channels, (iv) exiting from pores to membrane surface, and (v) diffusing from surface to the bulk permeate. It is reasonable to expect that the effect of concentration polarization is minor, if not completely negligible, under very low water flux. Thus, in the following discussion, a three-step model is proposed for ion transport through the zeolite membrane as illustrated in Figure 9: Step 1 is the ions entering the zeolitic pores from the bulk feed; Step 2 is ion diffusion from the feed side to the permeate side of the zeolite channel; and Step 3 is the ions exiting from the zeolite channels to the permeate solution. x_1 and x_2 are the ion mole fractions in the two ends of a zeolite channel. x_1 and x_2 are different from the ion compositions in the feed and permeate solutions because of the

selectivity at the zeolite pore openings [8,9] and possible electrostatic sorption of ions on the MFI (SiO₂) surface [10,11].

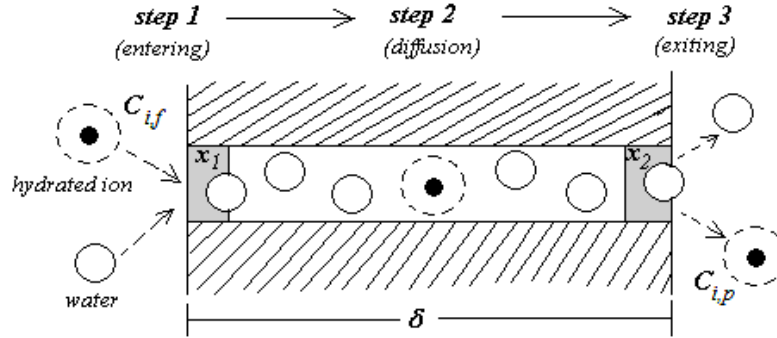


Fig. 9 Illustration of the three-step ion transport process through a zeolite channel.

Step 1 may also be considered as a lumped step, which includes the resistances for diffusion through the concentration polarization layer, if there is any, and the partial dehydration when entering the pores, which is likely the controlling factor. During RO permeation, hydrated ions first overcome the energy barrier to enter the zeolite channels. The energy barrier may be mainly determined by the energy required for partial dehydration during collision at the pore entrance (17). The net rate of ion entering the zeolite pores ($J_{i,l}$) is driven by the concentration difference between the feed solution ($C_{i,f}$) and inside pores near the membrane surface ($C'_{i,f}$):

$$J_{i,l} = K_l' \exp\left(\frac{-\Delta E_l}{RT}\right) \cdot (C_{i,f} - C'_{i,f}) \quad (5)$$

where K_l' is the lumped mass transfer coefficient including the ion population density at membrane surface for unity molality in feed and the effective frequency for ions to enter the pores; ΔE_l is the activation energy needed for ions to enter the zeolite pore.

The processes of ions entering and exiting the zeolite involve the exact same pathway but in reversed direction. Thus, the energy change associated with the exiting process is the negative value of ΔE_I . The rate of ions exiting the pores ($J_{i,3}$) in Step 3 is obtained:

$$J_{i,3} = K'_3 \exp\left(\frac{\Delta E_1}{RT}\right) \cdot (C'_{i,p} - C_{i,p}) \quad (6)$$

where K'_3 has the similar physical meaning as does K_I . Because the exiting ions are re-hydrated in the permeate and release energy, Step 3 is anticipated to be a fast process with an insignificant mass resistance compared to Step 1 [12].

In Step 2, ion diffusion through the membrane is driven by the concentration gradient along the zeolite channel, namely $dC'_i/d\delta (= [C'_{i,f} - C'_{i,p}]/\delta)$, where $C'_{i,f}$ and $C'_{i,p}$ are ion concentrations in the two ends of a zeolite channel on the feed and permeate sides, respectively. The ion diffusion rate in the zeolite channel (Step 2) can be described by the Fick's law equation,

$$J_{i,2} = D_{i,c} \frac{dC'_i}{d\delta} \approx D_{i,c}^0 \exp\left(\frac{-E_{i,c}}{RT}\right) \cdot \frac{C'_{i,f} - C'_{i,p}}{\delta} \quad (7)$$

where $D_{i,c}$ ($= D_{i,c}^0 \exp\{-E_{i,c}/RT\}$) is the ion diffusivity inside the zeolite channels. For dilute solutions, with negligible resistance in Step 3 (i.e. $C'_{i,p} \approx C_{i,p}$), the ion selectivity of Step 1 and 2 are given by the following eqs. (8) and (9), respectively:

$$\alpha_{i,1} \approx \frac{x_1}{x_f} \approx \frac{C'_{i,f}}{C_{i,f}} \quad (8)$$

$$\alpha_{i,2} \approx \frac{C'_{i,p}}{C'_{i,f}} = \frac{C_{i,p}}{\alpha_{i,1} \cdot C_{i,f}} = \frac{\alpha_i}{\alpha_{i,1}} \quad (9)$$

At steady state, the overall mass transport equation for ion through the membrane is obtained,

$$J_i = \frac{C_{i,f} - C_{i,p}}{\frac{1}{K'_1 \exp(-\Delta E_1 / RT)} + \frac{1}{D_{i,c} / \delta}} = \frac{r_i \cdot C_{i,f}}{\frac{1}{K'_1 \exp(-\Delta E_1 / RT)} + \frac{1}{D_{i,c} / \delta}} \quad (10)$$

Application of eq. (10) will require quantitative information on the interactions between ion, solvent, and zeolite surface at the pore entrance and inside the channels, which are currently not available. Because of the strong ion-water interactions in the zeolite channels, $D_{i,c}$ is affected by the water flux, which is a function of transmembrane pressure. The eq. (10) can be further simplified as

$$J_i = K_i \cdot r_i \cdot C_{i,f} \quad (11)$$

where $K_i (=1/[1/K'_1 \exp(-\Delta E_1 / RT) + \delta / D_{i,c}])$ (m/s) is the overall ion mass transfer coefficient through the membrane. If the rate determining step can be identified, eq. (11) can be used to estimate either the mass transfer coefficient for Step 1 or the ion diffusivity in the zeolite channels.

It has been demonstrated by the MD simulation (1) that Step 1 is rate determining for small pore PSZ membranes (e.g. ZK-4, dia. $\sim 4.1 \text{ \AA}$). However, on zeolite membranes of medium pore sizes, such as MFI (5.6 \AA) and Faujasite (FAU; 7.4 \AA), ions may be partially dehydrated by collision at the pore entrance to sizes small enough to enter the zeolite channels [9]. Furthermore, single-file diffusion was not found by MD simulations [7] for water and small cations in cylindrical channels similar to that of MFI zeolites. Therefore, the ion rejection and ion flow rate are anticipated to be determined by both Step 1, ions entering the pore entrances, and Step 2, ion diffusion in the MFI zeolite membranes.

Figure 10 shows the Arrhenius plots of the water and ion (Li^+ and Na^+) fluxes. The overall activation energies for permeation of Li^+ (ΔE_{Li^+}) and Na^+ (ΔE_{Na^+}) are 20.9 kJ/mol and

18.6 kJ/mol, respectively. The activation energies of water permeation (ΔE_w) were 11.2 kJ/mol and 9.7 kJ/mol for the 0.1 M LiCl and 0.1 M NaCl solutions, respectively. The permeation activation energy for ions (ΔE_i) is larger than that for water (ΔE_w), meaning that ion permeation is more sensitive to temperature compared to water. This is due mainly to the fact that raising the temperature increases the kinetic energy of hydrated ions and facilitates ion dehydration through collision at the zeolite pore entrances. It is known that the hydration numbers of alkali metal ions vary insignificantly with a modest change of temperature. The overall activation energy for Li^+ permeation, ΔE_{Li^+} , was greater than ΔE_{Na^+} because the charge density of Li^+ is higher than that of Na^+ . The number of tightly bound water molecules and the dehydration energy of a hydrated ion increase with its electrical charge density.

The overall mass transfer coefficients (K_i) of the alkali metal ions in the zeolite membranes at 50°C are estimated from the RO data by eq. (11). The membrane water permeability values for the corresponding solutions are estimated by eq. (4). The results are presented in Figure 11.

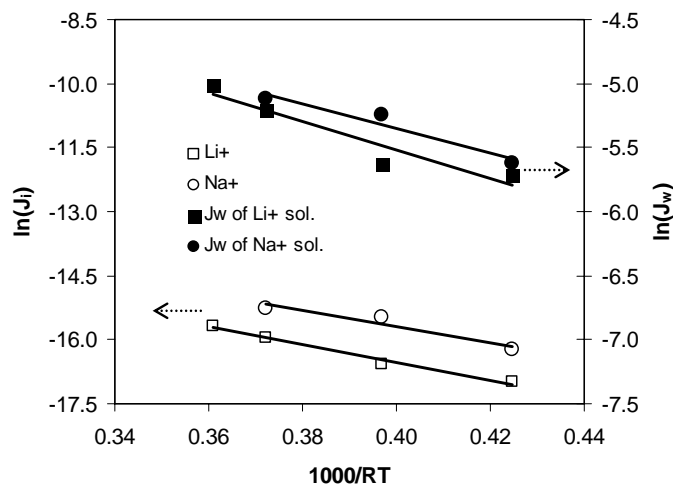


Fig. 10 Arrhenius plots of the water and ion fluxes for 0.10 M LiCl and 0.10 M NaCl solutions during RO.

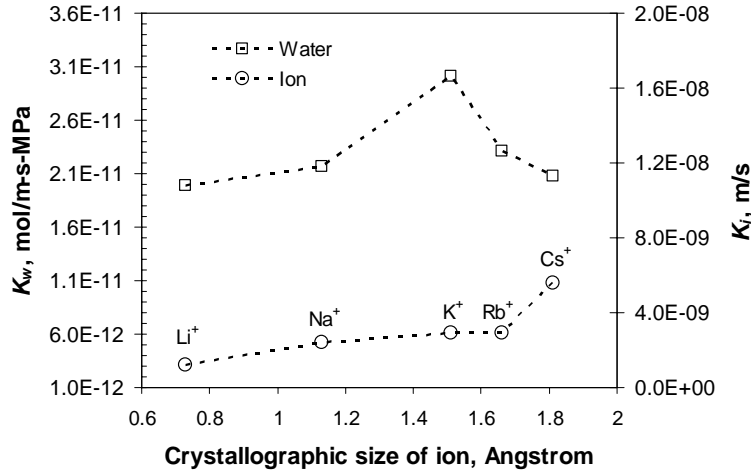


Fig. 11 Water permeability and overall ion transfer coefficient in the MFI membrane during RO at 50 °C as functions of crystallographic ion size.

The ion mass transfer coefficient through the zeolite membrane increased monotonically as a function of ion size, which followed the trend of the size-dependence of the ion mobility in bulk dilute solutions [7,13,14,15]. For the alkali metal ions, the water-ion bonding strength, and hence the solvation energy, decreases with increasing ion size. Thus, the energy required for ion dehydration decreases and the rate of ions entering the zeolite pores increases with ion size (16, 25). The ion diffusivity in the zeolite channels also increases as the number of tightly bounded water molecules decreases with ion size. On the other hand, computer simulations have shown that larger ions (Rb⁺ and Cs⁺) tend to depart from the center and stick to the pore wall more readily compared to the small size alkali metal ions (Li⁺, Na⁺ and K⁺) [9,16]. Thus, one would expect that the ion mobility in the zeolite channel increases in the order $D_{Li+,c} < D_{Na+,c} < D_{K+,c}$ as the charge density decreases but starts to decrease after K⁺ (for Rb⁺ and Cs⁺) [9]. The monotonic

relationship between the ion transfer coefficient and ion size suggests that ion permeation through the zeolite membrane is primarily determined by Step 1.

The water permeability, and hence its apparent mobility, in the zeolite membrane increased with the ion size and then decreased after a maximum at the 0.1M KCl solution. This suggests that the transport of the small water molecules through the membrane is mainly controlled by its diffusion rate in the zeolite channels but not the rate of entering the zeolite pores. The water diffusion rate is largely affected by the mobility of ions in the zeolite channels. For small ions like Li^+ , Na^+ , and K^+ , water molecules are able to pass the ions and the water diffusion rate increases with decreasing the water-ion bonding strength. However, as the ion size further increases (i.e. Rb^+ , dia. $\sim 3.3 \text{ \AA}$, and Cs^+ , dia. $\sim 3.6 \text{ \AA}$), the available space in the channel is reduced, which makes it more difficult for water molecules to surpass the ions in the zeolite channels (dia. $\sim 5.6 \text{ \AA}$).

The above discussion regarding the effects of ion charge density on ion and water transport in MFI membranes can also be supported by the results of a previous study on RO of 0.1 M chloride single-salt solutions containing Na^+ , Ca^{2+} , Mg^{2+} , and Al^{3+} (3). The ion rejection was found to increase with ion charge density in the order $\text{Na}^+ < \text{Ca}^{2+} < \text{Mg}^{2+} < \text{Al}^{3+}$, while the ion and water fluxes changed in the reverse order.

Effect of dissolved organics: In this study, permeation of DI water on the zeolite membrane was first carried out to study the water permeation without salt and organics. Then, RO separation tests on single-component solutions of 0.10 M NaCl solution and 500 ppm toluene solution were performed respectively. Finally, a binary solution containing 0.10 M NaCl and 500 ppm dissolved toluene was permeated through the zeolite membrane and rejection of both Na^+ and

toluene were tested by measuring their concentration changes in the feed and permeate solutions. The toluene concentration in the permeate solution was analyzed by a total organic carbon analyzer (TOC-VCPN) and ion concentrations were analyzed by IC (DX-120, without organics) and atomic adsorption (AA, with organics). Table 2 summarizes the separation results of these solutions together with the water flux of DI water.

Table 2. Influence of organics on the RO through MFI zeolite membranes

Solution	Water flux, Kg/m ² .h	Ion rejection, %	Toluene rejection, %
DI water	0.333	–	–
0.10 M NaCl	0.285	99.4	–
500 ppm toluene	0.016	–	99.5
0.10 M NaCl + 500 ppm toluene	0.018	77.8	99.8

The zeolite membranes shown very high separation efficiency (>99%) for single-component 0.10 M NaCl solution and 500 ppm toluene solution. The toluene rejection in the binary solution containing 0.10 M NaCl and 500 ppm toluene was virtually the same (99.8%) as that in 500 ppm single component solution (99.5%). However, the ion rejection decreased from 99.4% for the organic-free solution to 77.8% for solutions with dissolved toluene. The adsorption of organics in the zeolite membrane is responsible for the decline in ion separation efficiency.

Sensor for produced water management: Information on trace level dissolved organics in water with high temporal and spatial resolutions is highly demanded for effective produced water management. However, most of the existing approaches for trace detection of dissolved organics involve use of sophisticated instruments that require costly and time consuming sample

collection/preparation and laboratory analyses. In this research, we demonstrated a new type of zeolite-enabled optical fiber chemical sensors for in situ detection/monitoring of organics in water and gas phases [17,18]. The sensor comprised of a dense silicalite thin film grown on the straight cut endface of a standard telecommunication optical fiber (singlemode Corning SMF28[®], cladding diameter of 125 μ m with a 9- μ m core). The sensor operates based on measuring the change of refractive index of the zeolite film caused by adsorbing organic molecules into the zeolite structure [19]. This sensor will be applied to the RO demo unit to be delivered by the end of Phase III. Detailed information on the new sensors are provided in our recent publications [17-19].

2.4. Conclusions

During RO on zeolite membranes, the ion and water fluxes are enhanced simultaneously by increasing the temperature or the transmembrane pressure (ΔP). However, changing temperature and pressure have different impacts on the ion rejection rate. Raising the temperature has a greater influence on the ion permeation than on the water permeation, resulting in a decline of the ion rejection. On the contrary, increasing the transmembrane pressure can enhance both the water flux and ion rejection because the ion flux is much less affected compared to the water flux. The zeolite membranes were also found to have high rejection rates for dissolved organics during the RO process. However, the dissolved organics can cause decreases in ion rejection and water flux rates because of the adsorption of organic molecules in the zeolite pores. In the Phase II (Year 2) of the project, we will further optimize the operating conditions to enhance the RO performance for CBM produced water.

REFERENCES

1. X. Gu, J. Dong, T. M. Nenoff, D. E. Ozokwelu, Separation of *p*-Xylene from Multicomponent Vapor Mixtures Using Tubular MFI Zeolite Membranes. *J. Membr. Sci.*, revision submitted (2006).
2. X. Gu, J. Dong, T.M. Nenoff, Synthesis of defect-free FAU-type zeolite membranes and separation for dry and moist CO₂/N₂ mixtures. *Ind. Eng. Chem. Res.*, 44 (2005), 937 – 944.
3. X. Gu, J. Zhang, J. Dong, T.M. Nenoff, A Platinum-Cobalt-Loaded NaY Zeolite Membrane for Nonoxidative Conversion of Methane to Higher Hydrocarbons and Hydrogen. *Catal. Lett.*, 102, 1-2 (2005), 9 – 13.
4. L. Li, J. Dong, T.M. Nenoff, R. Lee, Desalination by Reverse Osmosis Using MFI Zeolite Membranes. *J. Membr. Sci.*, 243(2004) 401 – 404.
5. L. Li, J. Dong, T.M. Nenoff, R. Lee, Reverse Osmosis of Ionic Aqueous Solutions on A MFI Zeolite Membrane. *Desalination*, 170, 3(2004) 309 – 316.
6. L. Li, J. Dong, R. Lee, Preparation of alpha-alumina-supported mesoporous bentonite membranes for reverse osmosis desalination of aqueous solutions. *J. Colloid. Interf. Sci.*, 273 (2004), 540-546.
7. LyndenBell, R.M.; Rasaiah, J.C. Mobility and solvation of ions in channels. *J. Chem. Phys.* 1996, 105, 9266-9280.
8. Lin, J.; Murad, S. A computer simulation study of the separation of aqueous solution using thin zeolite membranes. *Molec. Phys.* 2001, 99, 1175-1181.
9. Andersen, O.S.; Feldberg, S.W. The heterogeneous collision velocity for hydrated ions in aqueous solutions is $\sim 10^4$ cm/s. *J. Phys. Chem.* 1996, 100, 4622-4629.
10. Nikolakis, V.; Tsapatsis, M.; Vlachos, D.G. Physicochemical characterization of silicalite-1 surface and its implications on crystal growth. *Langmuir* 2003, 19, 4619-4626.
11. Schreier, M.; Regalbuto, J.R. A fundamental study of Pt tetraammine impregnation of silica 1. The electrostatic nature of platinum adsorption. *J. Catal.* 2004, 225, 190-202.
12. Giaya, A.; Thompson, R.W. Water confined in cylindrical micropores. *J. Chem. Phys.* 2002, 117, 3464-3475.
13. Chong, S.; Hirata, F. Dynamics of Ions in liquid water: an interaction-site-model description. *J. Chem. Phys.* 1999, 111, 3654-3667.
14. Koneshan, S.; Lynden-Bell, R.M.; Rasaiah, J.C. Friction coefficients of ions in aqueous solution at 25 degrees C. *J. Am. Chem. Soc.* 1998, 120, 12041-12050.
15. Koneshan, S.; Rasaiah, J.C.; Lynden-Bell, R.M.; Lee, S.H. Solvent structure, dynamics, and ion mobility in aqueous solutions at 25 degrees C. *J. Phys. Chem. B.* 1998. 102, 4193-4204.
16. Bluhm, E.A.; Bauer, E.; Chamberlin, R.M.; Abney, K.D.; Young, J.S.; Jarvinen, G.D. Surface effects on cation transport across porous alumina membranes. *Langmuir*, 1999, 15, 8668-8672.
17. H. Xiao, J. Zhang, J. Dong, M. Luo, R. Lee, V. Romero, Synthesis of MFI zeolite films on optical fibers for detection of chemical vapors, *Optics Letters*, 30, 11(2005), 1270-1272.
18. J. Zhang, J. Dong, M. Luo, H. Xiao, S. Murad, R. A. Normann, Zeolite-Fiber Integrated Optical Chemical Sensors for Detection of Dissolved Organics in Water. *Langmuir*, 21 (2005), 8609-8612.
19. J. Zhang, M. Luo, H. Xiao, J. Dong, An Interferometric Study on the Adsorption-Dependent Refractive Index of Silicalite Thin Films Grown on Optical Fibers, *Chem. Mat.*, 18 (2006), 4 – 6.

PUBLICATIONS IN YEAR 1

Conference Presentations:

1. J. Dong, L. Li, H. Xiao, R. Lee, "Treating Coal-Bed Methane Produced Water for Beneficial Use By Reverse Osmosis through Zeolite Membranes", *Ground Water Protection Council (GWPC) Annual Meeting*, Portland, OR, September 24 – 28, 2005.
2. J. Zhang, H. Xiao, J. Dong, "Zeolite-Coated Optical Fiber Sensors for In-Situ Detection of Organics in Gas and Liquid Phases", *SPIE (the Intl. Soc. Opt. Eng.)*, Optics East, Boston, MA, October 23 –26, 2005.

Refereed Journal Publications:

3. L. Li, J. Dong, T.M. Nenoff, Transport of Alkali Metal Ions in MFI Zeolite Membranes during Reverse Osmosis. *To be submitted for publication* (2006).
4. X. Gu, J. Dong, T. M. Nenoff , D. E. Ozokwelu, Separation of *p*-Xylene from Multicomponent Vapor Mixtures Using Tubular MFI Zeolite Membranes. *J. Membr. Sci.*, revision submitted (2005).
5. J. Zhang, J. Dong, M. Luo, H. Xiao, S. Murad, R. A. Normann, Zeolite-Fiber Integrated Optical Chemical Sensors for Detection of Dissolved Organics in Water. *Langmuir*, 21 (2005), 8609-8612.
6. H. Xiao, J. Zhang, J. Dong. M. Luo, R. Lee, V. Romero, Synthesis of MFI zeolite films on optical fibers for detection of chemical vapors, *Optics Letters*, 30, 11(2005), 1270-1272.
7. X. Gu, J. Zhang, J. Dong, T.M. Nenoff, A Platinum-Cobalt-Loaded NaY Zeolite Membrane for Nonoxidative Conversion of Methane to Higher Hydrocarbons and Hydrogen. *Catal. Lett.*, 102, 1-2 (2005), 9 – 13.
8. X. Gu, J. Dong, T.M. Nenoff, Synthesis of defect-free FAU-type zeolite membranes and separation for dry and moist CO₂/N₂ mixtures. *Ind. Eng. Chem. Res.*, 44 (2005), 937 – 944.